Study on Composite Structure of Tian-Font Magnetic Shielding and Anti-Series Active Coils for Wireless Power Transfer System

Zhongqi LI, Wenjuan ZHANG, Ziyue GAN, and Bin LI

***Abstract*—In the wireless power transfer (WPT) system of electric vehicles, conventional magnetic shielding techniques usually rely on a large number of magnetic cores and aluminum plates, posing a cost challenge. To address this issue, this paper proposes a composite structure of Tian-font magnetic shielding and anti-series active coils to minimize material use while maintaining safe magnetic leakage levels. First, a calculation method of the magnetic field is introduced to analyze magnetic leakage in the target region of the system, providing a theoretical basis for optimization. Secondly, a composite shielding structure is introduced, its working principle is analyzed in detail and its circuit model is derived. Subsequently, a method for optimizing coil parameters is presented, and the optimal coil and shielding material parameters are determined. Finally, a WPT system based on this structure is built and verified through simulation and experiment. Results show that under a transmission power of 4 kW, the maximum magnetic leakage in the target region before and after offset is lower than 27 μT and the transmission efficiency is more than 93%. Compared to the same size, non-gouged magnetic shield structure, it saves 36.78% of the magnetic core and 32.52% of the aluminum plate.**

***Index Terms*—Active shielding, electric vehicle, leakage field, transmission performance, wireless power transfer.**

I. Introduction

With the deterioration of environmental problems and the dwindling of petroleum resources, electric vehicles have developed rapidly due to their green and emission-free features, and have become an important representative of modern transportation, receiving extensive attention from countries around the world [1], [2]. Electric vehicles with wireless power transmission (WPT) ensure safe charging even in extreme environments such as high temperatures and humidity, thanks to high operational safety, good waterproofing and easy maintenance [3]–[6]. However, the magnetic leakage that occurs during energy transmission in WPT systems not only interferes with the normal operation of the equipment but also poses potential risks to personnel safety [7], [8]. Therefore, in-depth investigation of magnetic shielding technology and its structural design in WPT systems has become an important part of current research in the field of wireless power transmission [9], [10].

Existing shielding methods can be classified into three main categories: passive shielding, reactive resonance shielding, and active shielding.

Passive shielding can be further divided into ferromagnetic core shielding and non-ferromagnetic metal shielding. Regarding the ferromagnetic core shielding method, Long T's team from the University of Cambridge took the lead in researching the application of nanocrystals in magnetic core shielding and found that nanocrystalline materials have excellent magnetic properties. However, the high conductivity characteristics of nanocrystalline materials can lead to significant eddy current losses, which affects the transmission efficiency of the magnetic core [11]. In contrast, traditional magnetic core shielding materials, while lacking exceptional magnetic properties, offer good transmission efficiency due to their low conductivity. To address this challenge, Zhang Wenting's team at the Hebei University of Technology developed a new type of composite magnetic core, which combines the superior shielding properties of nanocrystals with the transmission efficiency of traditional magnetic cores, thereby maintaining high shielding effectiveness while ensuring good transmission efficiency [12]. For the non-ferromagnetic metal shielding method, Zhu Qingwei's team at the Chinese Academy of Sciences used a whole aluminum plate to suppress magnetic leakage in the non-operating region, and the results showed that the suppression effect was significant. However, the whole aluminum plate reduces the system power and generates large eddy current losses under high-frequency and strong electromagnetic fields [13].

Manuscript received November 21, 2024; revised January 22, 2025; accepted February 16, 2025. Date of publication March 30, 2025; date of current version February 28, 2025. This work was supported by Scientific Research Fund of Hunan Provincial Education Department under the grant 23C0182, Excellent Youth Project of Scientific Research of Hunan Provincial Department of Education under the grant 22B0577, Key Projects of Hunan Provincial Department of Education under the grant 23A0432, National Key R&D Program Project under the grant 2022YFB3403200, National Natural Science Foundation of China (NSFC) Youth Science Fund Project under the grant 62303178, and Natural Science Foundation of Hunan Province under the grant 2022JJ30226. *(Corresponding author: Zhongqi Li.)*

Z. Li and W. Zhang are both with the College of Railway Transportation, Hunan University of Technology, Zhuzhou 412007, China (e-mail: 18750041055@163.com; my3eee@126.com).

Z. Gan and B. Li are both with the College of Electrical and Information Engineering, Hunan University of Technology, Zhuzhou 412007, China (e-mail: yueaa99@163.com; 3302757619@qq.com).

Digital Object Identifier 10.24295/CPSSTPEA.2025.00006

The shielding method of reactive resonance works similarly to non-ferromagnetic metal shielding, but it overcomes the power degradation associated with conventional metal shielding. The Korea Advanced Institute of Science and Technology (KAIST) team achieved significant suppression of magnetic leakage by the implementation of a self-tuning reactive current control system, which places a primary shielding coil adjacent to the coupling coils. However, the system did not achieve optimal performance [14]−[16]. To solve this problem, the team added a secondary shielding coil in a subsequent study to achieve optimal shielding [17]. Since the operating principle of reactive resonance shielding relies on the emitted magnetic field as a driver, the magnetic flux transmitted to the receiving coil may be reduced and, consequently, the coupling coefficient and the overall transmission efficiency of the system are adversely affected.

Aiming at the problem of system transmission efficiency degradation accompanied by the shielding method of reactive resonance in reducing magnetic leakage, the introduction of active shielding technology can improve the overall transmission performance of the system while realizing the effective suppression of magnetic leakage. Active shielding works by using a shielded coil with an excitation source to generate a counteracting magnetic field opposite to the original leaking field [18]. The method of reducing the magnetic leakage of a system by dividing the active shielding loop into two separate half-toroidal shielding coils was proposed by scholars such as Campi,et al.. Although changing the shape of the traditional active coil reduces the magnetic field next to the active coil, it fails to effectively improve the overall magnetic leakage shielding effect of the system [19]. Based on the use of multi-coil active shielding technology, the team proposed a new shielding structure, which added rectangular magnetic cores and aluminum plates at the transmitter and receiver ends to improve transmission efficiency, but this method also led to an increase in the overall size of the system [20].In active shielding design, the addition of secondary coils can have various effects on the main circuit. Lee and other scholars proposed a novel coil structure that combines a shielding coil to reduce magnetic leakage and an amplifying coil to enhance magnetic field strength. Through experimental optimization of coil size and turn count, they achieved effective suppression of magnetic leakage. However, its additional shielding coil inevitably increases the circuit complexity and reduces the transmission efficiency [21]. Mi M and other scholars proposed a dual-loop active shielded coil design, which directly connects the shielding coil in series with the transmitting coil, eliminating the additional coupling between the shielding coil and the receiving coil [22]. However, this design used a complete magnetic core and an aluminum plate as materials, which not only led to an increase in cost, but also significantly reduced the transmission efficiency of the system when the positions of the transmitting and receiving coils were shifted [23]. Therefore, the current difficulty lies in the design of a magnetic shielding structure that meets safety standards for magnetic leakage, ensures high transmission efficiency, and saves on the use of shielding materials as much as possible.

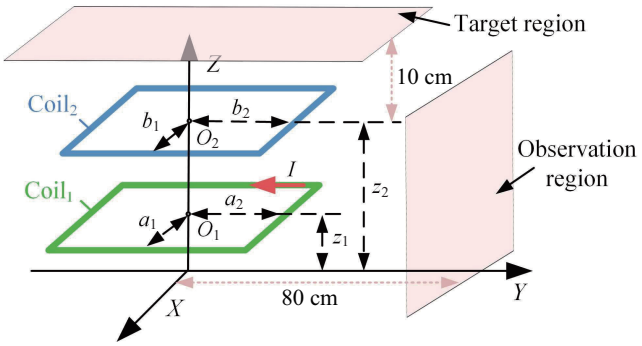

Fig. 1. Schematic diagram of rectangular coil structure.

In this paper, a composite structure of Tian-font magnetic shielding and anti-series active coils(TMSAC) is proposed, which has the same receiving and transmitting ends, including a Tian-font magnetic core and a Tian-font aluminum plate outside the main coil and an active shielding coil in anti-series with the main coil. The combination of the high permeability of the magnetic core and the conductivity of the aluminum plate reduces most of the magnetic leakage, improves the transmission efficiency, and reduces the cost of the Tian-font structure compared to a complete shielding material. Anti-series active shielding technology provides additional conditioning capability and reduces leakage at specific locations. Based on this, the structure can realize the magnetic shielding effect with high efficiency, economy, and compliance with safety standards. The rationality of the proposed method and structure is fully verified by comparing the theoretical, simulated, and experimental values. The experimental results show that the proposed shielding structure reduces the magnetic leakage by 88.23% without additional power. Saving 36.78% of the magnetic core and 32.52% of the aluminum plate compared to the magnetic shielding structure with the same size and without dug holes, the transmission efficiency can reach 95.83%.

II. TMSAC Structure

A. Calculation of Coil Magnetic Induction Strength

Rectangular coils are employed in this structure, and in order to calculate the magnetic field distribution in the space, a method for calculating the magnetic induction strength of rectangular coils based on vector magnetic potential is introduced in this section[24],[25]. Fig. 1 shows a schematic structure of Coil_1 and Coil_2.

Regarding the rectangular coil shown in Fig. 1, a_1 and a_2 represent the half-length and half-width of Coil_1 , b_1 and b_2 represent the half-length and half-width of Coil_2, respectively, and z_1 and z_2 denote the distances from Coil_1 and Coil_2 to the Y-axis, respectively. In addition, an arbitrary point $P(x, y, z)$ is set in the structure with the vector magnetic potential expression:

$$A(x,y,z) = \frac{\mu_0}{4\pi} \int_{v'} \frac{J(x',y',z')\mathrm{d}v'}{R} \tag{1}$$

where J denotes the current density, v denotes the current distribution in Coil_1, R is the distance between any point $P(x, y, z)$ to the point source (x', y', z'). Based on the vector magnetic potential, the flux density B_i expression can be obtained as:

$$B_i = \nabla \times A = a_x\left(\frac{\partial A_z}{\partial y}-\frac{\partial A_y}{\partial z}\right) + a_y\left(\frac{\partial A_x}{\partial z}-\frac{\partial A_z}{\partial y}\right) + a_z\left(\frac{\partial A_y}{\partial x}-\frac{\partial A_x}{\partial y}\right) \tag{2}$$

The magnetic flux density B_i is resolved along the X-axis, Y-axis, and Z-axis directions in the three-dimensional space in which it is located to obtain the expressions for the components of the magnetic induction B_i, respectively:

$$B_x=\frac{1}{4\pi^2}\int_{-\infty}^{\infty}\int_{-\infty}^{\infty} b_x \cdot e^{j(x\xi+y\eta)}\mathrm{d}\xi\mathrm{d}\eta \tag{3}$$

$$B_y=\frac{1}{4\pi^2}\int_{-\infty}^{\infty}\int_{-\infty}^{\infty} b_y \cdot e^{j(x\xi+y\eta)}\mathrm{d}\xi\mathrm{d}\eta \tag{4}$$

$$B_z=\frac{1}{4\pi^2}\int_{-\infty}^{\infty}\int_{-\infty}^{\infty} b_z \cdot e^{j(x\xi+y\eta)}\mathrm{d}\xi\mathrm{d}\eta \tag{5}$$

Among them:

$$b_x=\frac{-j2\mu_0 I\sin(\xi a_1)\sin(\eta a_2)}{\eta}\cdot e^{(s_1-z)k} \tag{6}$$

$$b_y=\frac{-j2\mu_0 I\sin(\xi a_1)\sin(\eta a_2)}{\xi}\cdot e^{(s_1-z)k} \tag{7}$$

$$b_z=\frac{-2\mu_0 Ik\sin(\xi a_1)\sin(\eta a_2)}{\xi\eta}\cdot e^{(s_1-z)k} \tag{8}$$

In the above equation, ξ and η are double Fourier integral variables. Thus, the magnetic induction B can be expressed as:

$$B=\sqrt{B_x^2+B_y^2+B_z^2} \tag{9}$$

The magnetic induction strength calculations presented in this section provide the theoretical basis for the leakage optimization below.

B. Analysis of the TMSAC Structure

The key feature of the TMSAC structure is its combination of a Tian-font design with an anti-series active shielding coil. Magnetic cores are selected as shielding materials, greatly improving the transmission efficiency of the system, however, the magnetic leakage problem of the system remains significant. While an aluminum shielding layer effectively reduces magnetic leakage, it also decreases the coupling coefficient. To address this issue, this design combines magnetic cores with aluminum plates, thus integrating the benefits of each material to enhance coupling efficiency, reduce magnetic leakage, and optimize overall system performance. Based on the selection of shielding materials, this section will conduct a specific analysis of the Tian-font magnetic core and aluminum plate, as well as the anti-series active shielding design.

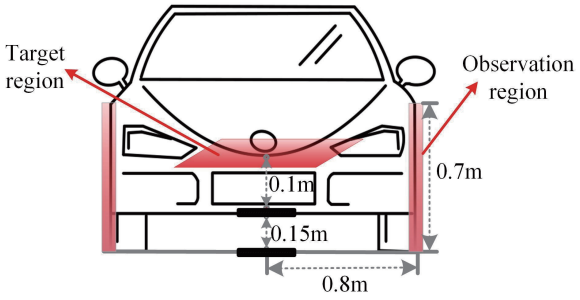

Fig. 2. Schematic diagram of the magnetic leakage target region and observation region.

The material digging is simulated using the Ansys Maxwell simulation tool based on the finite element method, with evaluation metrics including the coupling coefficient of the system and maximum magnetic leakage from the target region. The coupling coefficient k, a key concept in electromagnetic field theory, measures the electromagnetic shielding effect and is defined as follows:

$$k=\frac{M}{\sqrt{L_1 L_2}} \tag{10}$$

where M represents mutual inductance, and L_1 and L_2 are the self-inductances of Coil_1 and Coil_2 , respectively.

For the vertical magnetic leakage standard, according to the electric vehicle wireless charging standard GB/T 38775 part 4 safety specification, the vertical height of 70 cm outside the car is set as the demarcation line, and the leakage magnetic field strength in it and above should be controlled within the safety range value of 27 μT. For the leakage magnetic standard in the horizontal direction, following the specification of SAEJ2954 standard on the evaluation of leakage magnetic field of electric vehicles, the selected measurement area of the leakage magnetic field is 80 cm from the center point of the charging coil and 70 cm from the height of the ground, and the strength of the leakage magnetic field should be within the value of 6.25 μT, and in this paper, the area is set up as the observation region. By using a combined magnetic core and aluminum plate shielding material, the proposed design effectively suppresses horizontal magnetic leakage, keeping it well below the safety threshold on the observation region. Therefore, the study focuses on leakage levels 10 cm directly above the system, corresponding to the EV's internal magnetic leakage, the area is set up as the target region. Schematic diagram of the magnetic leakage target region and observation region as illustrated in Fig. 2.

When creating holes in the cores and aluminum plates, parameters such as hole size, coil, and material dimensions are kept consistent to ensure fairness and accuracy in performance comparisons. The coupling coefficients and maximum magnetic leakage at the target region for four types of structures are presented in Table I: type I (no holes in the magnetic core and

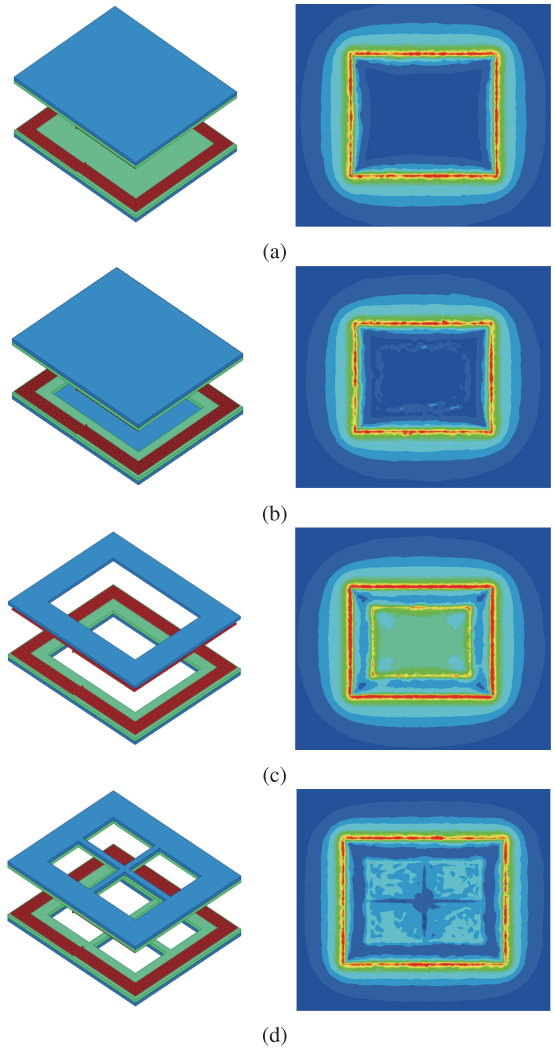

Fig. 3. Simulation models of four types and their magnetic field distribution diagrams. (a) No holes in the magnetic core and aluminum plate. (b) Single-hole magnetic core with full aluminum plate. (c) Single-hole magnetic core with single-hole aluminum plate. (d) Tian-font magnetic core with Tian-font aluminum plate.

TABLE I
COMPARISON OF THE PERFORMANCE OF FOUR TYPES

Type	k	B_{max}/μT	Savings/%
I: No-hole Core+Al Plate	0.23	47.84	—
II: Single-hole Core+Full Al Plate	0.17	46.88	21.55
III: Single-hole Core+Single-hole Al Plate	0.18	55.61	43.10
IV: Tian-font Core+Tian-font Al Plate	0.21	45.77	38.21

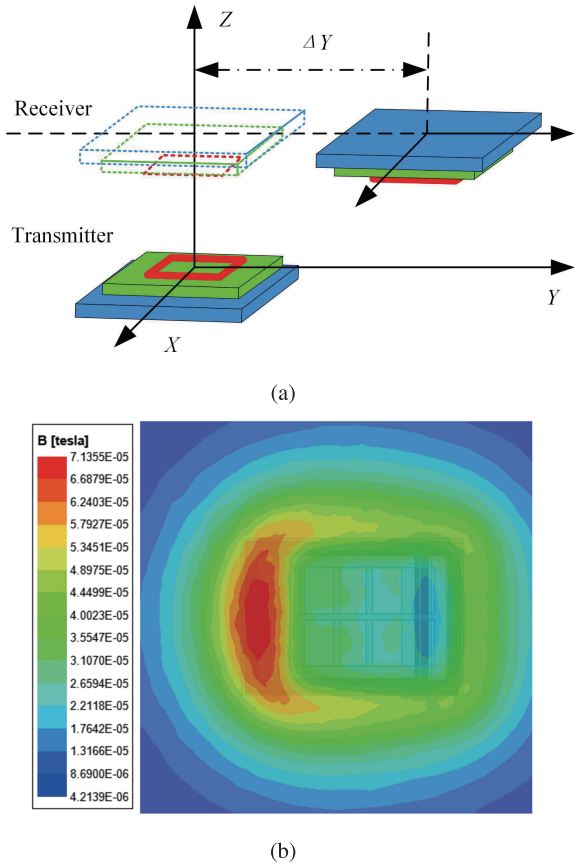

Fig. 4. Post-offset schematic diagram, target region magnetic field map. (a) Schematic diagram after offset. (b) Target region magnetic field map.

aluminum plate), type II (single-hole magnetic core with full aluminum plate), type III (single-hole magnetic core with single-hole aluminum plate), and type IV (Tian-font magnetic core with Tian-font aluminum plate). The Tian-font represents the shape of a whole board after digging four holes, as shown in Fig. 3(d). The data in Table I are further analyzed as follows.

Cut holes can effectively reduce the volume of the core and aluminum plate, thus reducing the manufacturing cost of the system. Type I is the case where there is no gouge and can be compared with other types. Due to the reduction in the effective volume of the core material in type II, the ability to limit magnetic leakage is reduced. Since the permeability of the core directly affects the magnetic coupling, a decrease in permeability weakens the coupling. Table I shows that the coupling coefficient of type II is reduced by 0.06 compared to type I, while the leakage is reduced by only 2.00%. In type III, perforating the aluminum plate reduces its effective coverage area, resulting in poor shielding in certain regions. As a result, the magnetic leakage increases by 18.62% compared to type II with an all-aluminum plate. However, the coupling coefficient increased by 0.01 and the material usage decreased by 43.10%.

Type IV saves shielding material while maintaining a high coupling coefficient. Observing the magnetic field distribution in Fig. 3, it can be seen that the field distribution of the Tian-font type design is more uniform than that of the single-hole structure. The magnetic leakage at the target region decreases from 55.61 to 45.77 μT, indicating that strategically placed holes effectively reduce magnetic leakage while saving material. Considering both material savings and shielding performance, the Tian-font design has significant advantages.

Fig. 4 illustrates the schematic of the system after a 10 cm

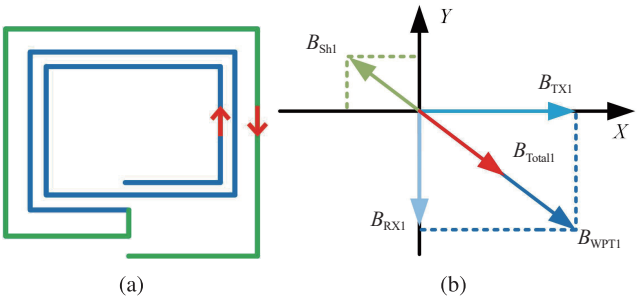

Fig. 5. Schematic diagram of anti-series active shielding. (a) Active shielded coil structure. (b) Schematic of magnetic field vector superposition.

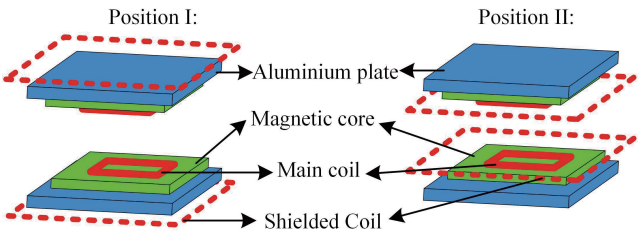

Fig. 6. Schematic diagram of two positions of shielding coils.

offset along the positive *Y*-axis, along with the magnetic field distribution in the target region. The analysis proceeds as follows:

For the shielding structure with the combination of a magnetic core and aluminum plate, the magnetic leakage can be effectively reduced when no offset occurs. However, when analyzing the magnetic field distribution characteristics after offset, it can be observed that the maximum magnetic leakage at the target region after offset rises from 45.77 to 71.36 μT due to the influence of the flux at the exposed transmitter side after offset, and the magnetic leakage increases significantly. Considering that the method of metal shielding leakage is limited by factors such as cost and construction in practical applications, this design introduces an anti-series active shielding coil on the outside of the structure, aiming at further suppressing the leakage through the structural design of this coupling mechanism. As shown in Fig. 5, the active shielding coil is coupled in reverse series with the original coil, generating a magnetic field that is opposite to the original magnetic field, thereby reducing magnetic leakage. To streamline circuit design, the shielding coil is integrated into the main WPT circuit, enabling it to share the same excitation source.

To determine the optimum shielding position of active shielding coil in the vertical direction, as shown in Fig. 6, active shielding positions I and II indicate the shielding coil outside and inside the main coil, respectively, were compared and their effects were analyzed. The same number of turns and other parameters of the shielding coil were placed in the two positions to ensure the fairness and accuracy of the performance comparison. $B_{max}{}^{1}$ and $B_{max}{}^{2}$ in Table II indicate the maximum value of magnetic leakage at the target region before and after the offset, respectively.

A schematic diagram in the cross-section of the shielding structure is shown in Fig. 7. Position II allows the magnetic circuit generated by the shielding coil to join the main magnetic chain within the coupling region, making the total effective magnetic coupling weaker. This results in a lower mutual inductance between the transmitter and receiver, which decreases the maximum pickup voltage of the load and reduces the maximum transmitted power of the system. As indicated in Table II, position II exhibits a lower coupling coefficient than position I, which has minimal impact on the coupling coefficient. Additionally, the maximum leakage after offset at positions I and II is 66.71 and 69.13 μT, respectively, demonstrating that the shielding coil effectively reduces magnetic leakage in the target region. Leakage remains higher in position II than in position I, both before and after offset. Therefore, for an anti-series active shielding design, the shielding coil should avoid the main coupling magnetic circuit and be positioned at position I. To place the active shielding coil below the target region while avoiding the main magnetic circuit, it should be located outside the transceiver structure on both sides, adjacent to the aluminum plate. In summary, the schematic of the final structure of the TMSAC is shown in Fig. 8.

TABLE II
COMPARISON OF THE PERFORMANCE OF TWO POSITIONS

Position	k	$B_{max}{}^{1}$/μT	$B_{max}{}^{2}$/μT
I: Outside the main coil	0.20	42.01	66.71
II: Inside the main coil	0.13	43.39	69.13

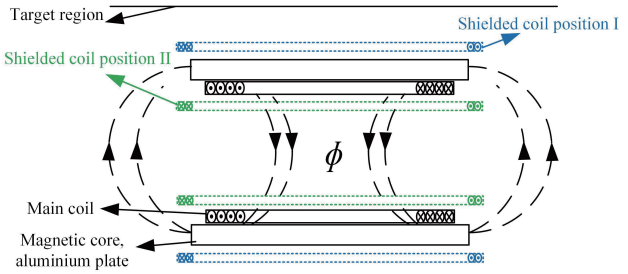

Fig. 7. Schematic diagram of shielding structure in cross-section.

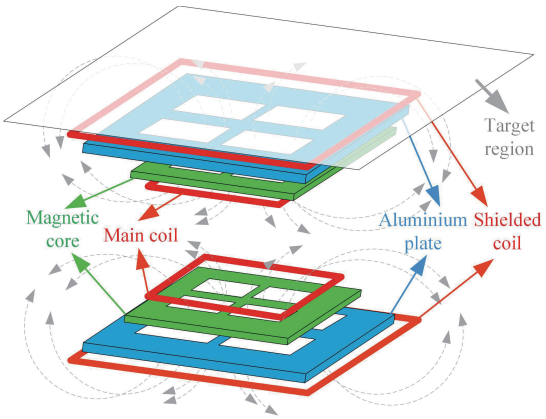

Fig. 8. Structure of the TMSAC.

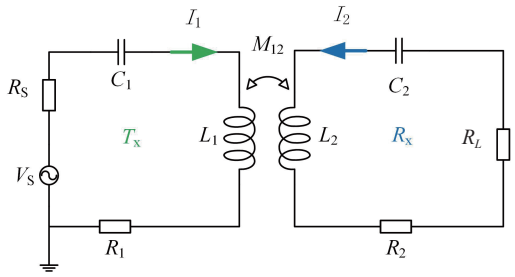

Fig. 9. Equivalent circuit model of coil.

C. Mathematical Model

Based on the rectangular coil of the TMSAC structure, the equivalent circuit can be modeled as shown in Fig. 9. The equivalent circuit of the coil can be represented as two loops with coils, where T_X represents the transmitting coil and R_X represents the receiving coil. The parameters of transmitting coil include the resonant capacitance (C_1), the self-inductance (L_1), and the equivalent resistance (R_1), while the internal resistance of the power supply (V_S) is R_S. The parameters of the receiving coil include the resonant capacitance (C_2), the self-inductance (L_2), and the equivalent resistance (R_2), and the mutual inductance between the coils is denoted by M_{12}. Based on this equivalent circuit model, the corresponding Kirchhoff voltage equation matrix can be established as follows:

$$\begin{bmatrix} Z_1 & j\omega M_{12} \\ j\omega M_{12} & Z_2 \end{bmatrix} \begin{bmatrix} I_1 \\ I_2 \end{bmatrix} = \begin{bmatrix} V_S \\ 0 \end{bmatrix} \tag{11}$$

Since the structure operates under resonant conditions, the impedance of the transmitting and receiving coils can be expressed as $Z_1 = R_1 + R_S$ and $Z_2 = R_2 + R_L$. Therefore, the specific expressions for the currents I_1 and I_2 can be derived as follows:

$$\begin{cases} I_1 = \dfrac{Z_2 V_S}{Z_1 Z_2 + (\omega M_{12})^2} \\ I_2 = -\dfrac{j\omega M_{12} V_S}{Z_1 Z_2 + (\omega M_{12})^2} \end{cases} \tag{12}$$

An expression for the transmission efficiency can be obtained from (12):

$$\eta = \left| \frac{I_2^2 R_L}{V_S I_1} \right| = \left| -\frac{(\omega M_{12})^2 R_L}{Z_1 Z_2^2 + (\omega M_{12})^2 Z_2} \right| \tag{13}$$

Bringing the impedance values $Z_1 = R_1 + R_S$ and $Z_2 = R_2 + R_L$ into (13), the transmission efficiency is obtained as follows:

$$\eta = \frac{(\omega M_{12})^2 Z_2}{(R_1+R_S)(R_L+R_2)^2 + (\omega M_{12})^2 (R_L+R_2)} \tag{14}$$

By deriving the R_L, the optimal load expression for this structure at maximum transmission efficiency can be obtained as follows:

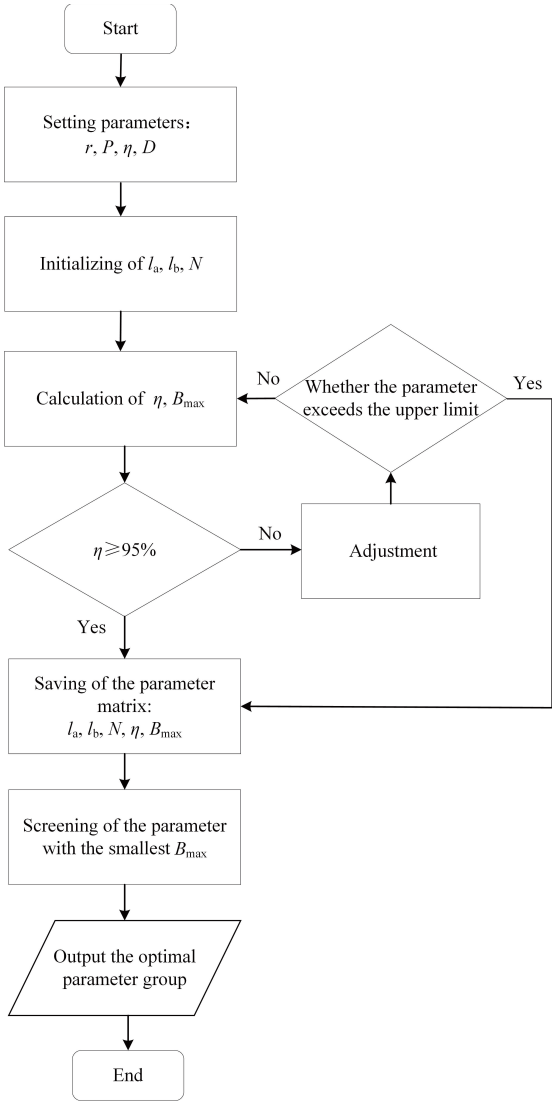

Fig. 10. Flow chart of main coil optimization.

$$R_{opt} = \sqrt{\frac{(R_1+R_S)^2 + (\omega M_{12})^2 R_2}{R_1 + R_S}} \tag{15}$$

III. Optimization of the TMSAC Structure

A. Optimization of the Main Coil

For the optimization of the main coil, the design uses the magnetic induction strength calculation and the transmission efficiency calculation. The two important parameters, the transmission efficiency (η) and the maximum magnetic leakage (B_{max}) are both affected by the coil's inner diameter size and the number of winding turns. Based on this, an optimization strategy is designed to find out the optimal parameters with efficiency higher than 95%. The flow chart of optimization is illustrated in Fig. 10, and its details are described below.

(1) Setting of parameters: Leeds copper wire with a diameter (r) of 0.39 cm was selected, the output power (P) was set to

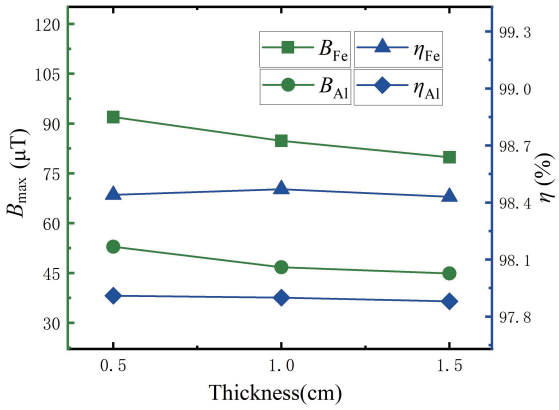

Fig. 11. Distribution diagram of magnetic leakage and transmission efficiency when the different thicknesses of the magnetic core and aluminum plate.

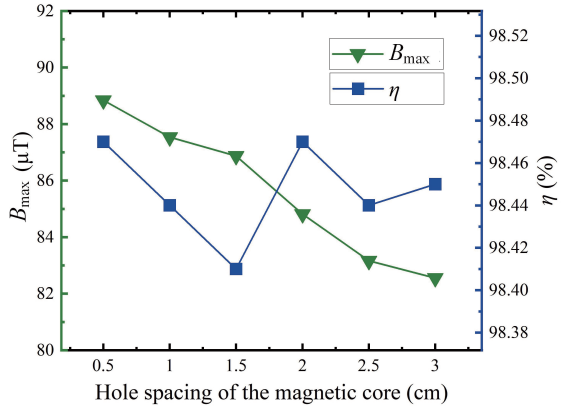

Fig. 12. Distribution diagram of system magnetic leakage and transfer efficiency when magnetic core intervals are different.

4 kW, the transmission efficiency (η) was set to 95%, and the transmission distance (D) between the transmitting and receiving coils was set to 15 cm.

(2) Initialization settings: the inner length (l_a) of the transmitting and receiving coils was adjusted within the range of 10 to 26 cm in steps of 1 cm, and the inner width (l_b) was similarly configured between 10 and 26 cm in steps of 1 cm, in addition, the number of turns (N) of the transmitting and receiving coils was set between 11 and 16 turns in steps of 1 turn.

(3) Calculate the coil transmission efficiency (η) and the maximum magnetic leakage (B_{max}) of the observation region: the transmission efficiency is obtained by (13) and (14), and the range of the observation region is set as follows: X-axis (–100 cm, 100 cm), Y-axis (80 cm), and Z-axis (0 cm,70 cm), and the distribution of magnetic leakage of the observation region can be obtained in Matlab according to (1) to (9).

(4) Screening for transmission efficiency: the transmission efficiency calculated for each parameter group is compared and screened. If the transmission efficiency $\eta \geqslant 95\%$, the parameter group is retained in the parameter matrix; if this criterion is not reached, the optimization of coil parameters continues. When the optimization reaches the upper limit of the preset parameters, the optimization procedure is terminated and proceeds to the next step.

(5) Screening of magnetic leakage: To realize the optimal magnetic shielding performance while ensuring higher transmission efficiency, the parameter group with the smallest B_{max} is selected at this stage from the parameter groups that satisfy the transmission efficiency criteria retained in the previous round of screening.

(6) Output the optimal parameter group: the parameters output after screening are the optimal parameters optimized to balance high efficiency and optimal shielding performance.

The final coil parameters obtained are: l_a is 48 cm, l_b is 38 cm, N is 11 turns, and the parameter of the two coils are consistent.

B. Optimization of Magnetic Cores and Aluminum Plates

The optimization of magnetic cores and aluminum plates involves two steps: adjusting their thickness and configuring the dug-hole dimensions. For thickness optimization, magnetic cores and aluminum plates are evaluated at three thicknesses: 0.5, 1, and 1.5 cm. A thicker magnetic core can support higher currents without magnetic saturation but raises material costs and weight. Here, B_{Fe} and B_{Al} represent magnetic leakage at the different thicknesses of the magnetic core and aluminum plate, respectively. Moreover, η_{Fe} and η_{Al} represent the transmission efficiency with different thicknesses of the magnetic core and aluminum plate, respectively. Simulation results in Fig. 11 show that magnetic leakage in the target region decreases as core thickness increases, but transmission efficiency peaks at 1 cm thickness. Given the cost implications of increased thickness, a 1 cm magnetic core thickness is selected. The aluminum plate is added based on the magnetic core shielding and the thickness of the aluminum plate is changed showing minimal effect on transmission efficiency, with only a slight loss to the system. However, magnetic leakage decreases gradually as thickness increases. Since the 1 and 1.5 cm thicknesses of the aluminum plate provide similar leakage reduction, a 1 cm thickness is chosen to balance weight and cost.

The second optimization step involves configuring the size of the dug holes. The size of the inner diameter of the main coil limits the size of the magnetic core and aluminum plate dug holes, according to the optimal parameters of the main coil in the previous section, it is concluded that the design of the dug holes will be set to be carried out based on the rectangular shape of 35 cm × 45 cm.

In this rectangle should first determine the middle spacing of the four holes: if too narrow, magnetic leakage will intensify in the middle, while excessive spacing impacts material savings. Considering six widths as shown in Fig. 12, the four holes are evenly distributed, and it can be seen that the magnetic core leakage decreases as the spacing increases, when the spacing is 2 cm, not only the leakage magnetic is lower, but also the efficiency second only to the spacing is 0.5 cm. Therefore, the intermediate spacing of 2 cm for the magnetic core is adopted

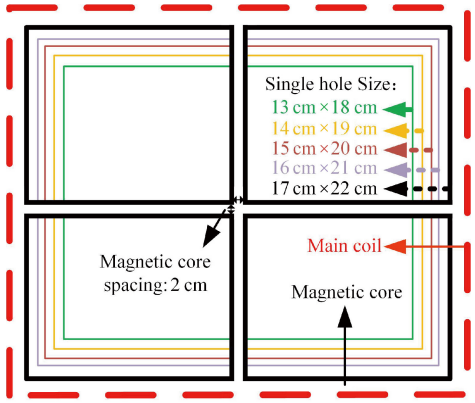

Fig. 13. Schematic diagram of magnetic core digging.

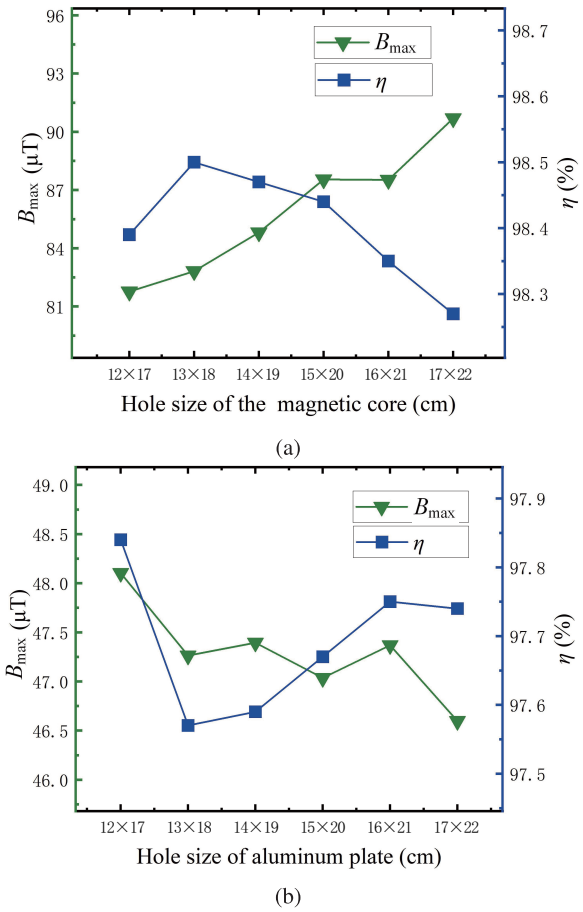

Fig. 14. Distribution diagram of system magnetic leakage and transmission efficiency when the holes are different. (a) Magnetic core. (b) Aluminum plate.

in this paper, and the intermediate spacing of 2 cm for the aluminum plate is also adopted in consideration of the support of shielding material, based on which the dimensions of single holes of the magnetic core and the aluminum plate are considered.

To maximize material savings, the dug holes should be as large as possible within the limits of the shielding coil's inner diameter, so consider the magnetic core hole size of six types, the length and width of the step are 1 cm, about the digging holes schematic diagram as shown in Fig. 13, the four holes of

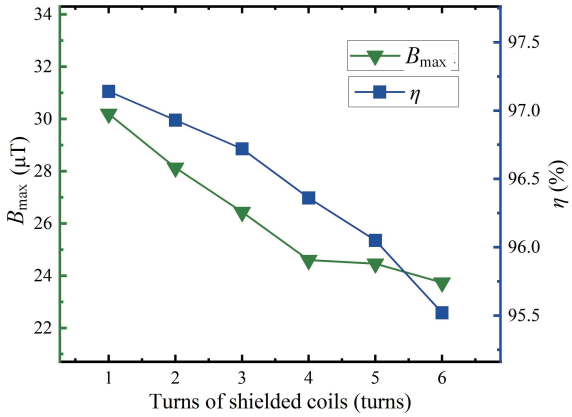

Fig. 15. Distribution diagram of transmission efficiency and magnetic leakage with different numbers of turns.

the same size and uniform distribution. From the simulation results in Fig. 14(a), it can be seen that the magnetic leakage of the single hole size 15 cm × 20 cm and 16 cm × 21 cm is almost the same. Although the transmission efficiency of a single hole size of 15 cm × 20 cm is lower, the volume saved by the single hole 16 cm × 21 cm is more. So, the magnetic core single hole size 16 cm × 21 cm is chosen to save the volume of 13.44 cm^3.

Based on the determination of the magnetic core hole size, the effect of the aluminum plate hole size on magnetic leakage and transmission efficiency is analyzed. As shown in Fig. 14(b), magnetic leakage is minimized when the aluminum plate hole size is 17 cm × 22 cm. Under this configuration, the transmission efficiency is similar to that of the 16 cm × 21 cm hole size, but more volume is saved. Therefore, the final chosen size for the aluminum plate hole is 17 cm × 22 cm, saving 14.96 cm^3 of volume.

C. Optimization of Active Shielded Coils

The magnetic induction calculation formula presented in (1) applies only to energized wires, but the actual system is subject to interference from the complex magnetic field of the EV body and the surrounding environment. Thus, the optimization of the active shielding coil needs to be modeled with the help of a finite element simulation platform. Increasing the number of turns in the active shielding coil can enhance the electromagnetic shielding effect. However, it also increases the coil's resistance, requiring more current to generate the same electromagnetic field strength, which in turn raises power consumption and design complexity. This results in a trade-off between shielding effectiveness and power efficiency when selecting the number of coil turns.

The effect of the number of shielding coil turns on the shielding effectiveness and transmission efficiency is analyzed. Fig. 15 shows the maximum magnetic leakage after offset for six different turn configurations. As the number of turns increases, shielding effectiveness improves, but transmission efficiency decreases. The reduction in magnetic leakage slows down after four turns. Therefore, the optimal number of turns for the active shielding coil is selected to be four.

TABLE III
PARAMETERS OF COIL

Coil	Inner length/cm	Inner width/cm	Turns
T_x	48.00	38.00	11
S_{Tx}	73.80	63.80	4
R_x	48.00	38.00	11
S_{Rx}	73.80	63.80	4

TABLE IV
PARAMETERS OF MAGNETIC CORE AND ALUMINUM PLATE

cm

Materials	Dimension of each material				
	Outer length	Outer width	Single hole length	Single hole width	Thickness
Tx_{Fe}	63.00	58.00	21.00	16.00	1.00
Tx_{Al}	73.00	63.00	22.00	17.00	1.00
Rx_{Fe}	63.00	58.00	21.00	16.00	1.00
Rx_{Al}	73.00	63.00	22.00	17.00	1.00

D. The Result of Optimization

The main coil size parameters are obtained according to Section II-A, and the parameters related to the shielding structure are obtained according to Section II-B. In the vertical position, outside the main coil are the magnetic core, aluminum plate, and shielding coil, and the four holes are spaced 2 cm apart from each other.

Based on the above, the optimal plate sizes of the magnetic core and the aluminum plate are found so that the maximum magnetic leakage after offset is below 27 μT to ensure that the safety leakage standard is met. The specific coil parameters, core, and aluminum plate parameters are shown in Tables III and IV, respectively. In Table III, T_x and S_{Tx} denote the main and shielded coils at the transmitter end, and R_x and S_{Rx} denote the main and shielded coils at the receiver end, while Tx_{Fe} and Tx_{Al} denote the core and the aluminum plate at the transmitter end, and Rx_{Fe} and Rx_{Al} denote the core and the aluminum plate at the receiver end, as shown in Table IV.

The magnetic shielding model at the optimal parameters of the TMSAC structure is simulated to obtain the self-inductances L_1 and L_2, internal resistances R_1, R_2, and mutual inductance M_{12}, which are substituted into (14) to obtain the transmission efficiency of the system after offsetting as 96.61%. According to (15), the optimal load corresponding to the parameters of the magnetic shield structure is obtained as 24.00 Ω.

To clearly show the advantage of the TMSAC structure in leakage magnetic shielding, the magnetic field distribution diagram after a 10 cm offset of the target region unshielded structure and the TMSAC structure are compared and analyzed. As shown in Fig. 16, it can be seen that the TMSAC structure reduces the maximum magnetic leakage of the unshielded structure by 85.62% after a 10 cm offset, which saves material aluminum by 32.52% and magnetic core by 36.78%. This comparison shows that the TMSAC structure can effectively suppress the magnetic leakage on the target region while optimizing the use of materials, which demonstrates its remarkable shielding performance.

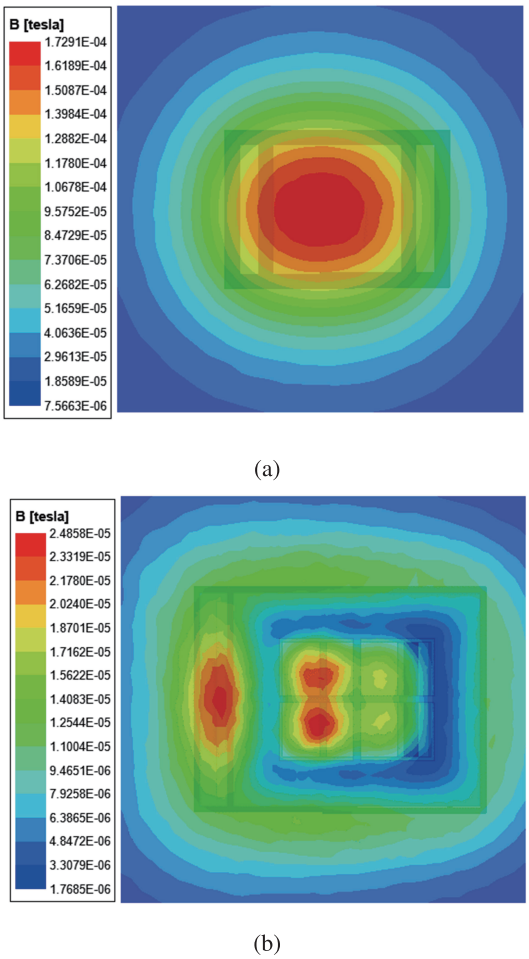

Fig. 16. Magnetic field distribution diagram at the target region after offsetting the unshielded structure and the TMSAC structure. (a) Unshielded structure. (b) TMSAC structure.

IV. EXPERIMENTAL VERIFICATION

In order to verify the effectiveness of the proposed structure and its optimization strategy, a set of 4 kW experimental verification platforms is constructed, the main components of which are RT-unit inverter-rectifier module, oscilloscope, DC power supply, a set of experimental main body consisting of the main coil, shielded coil, magnetic core, aluminum plate and load, as well as the measurement equipment, NF-5035S EMF analyzer, WT5000 power analyzer and IM3536 impedance analyzer. The DC power supply first generates a high-frequency square wave through the inverter module, which drives the transmitting coil to generate a high-frequency magnetic field. Subsequently, the receiving coil receives and converts this magnetic field into electrical energy, which is processed by the rectifier module to provide stable power to the load. All the coils in Table III are

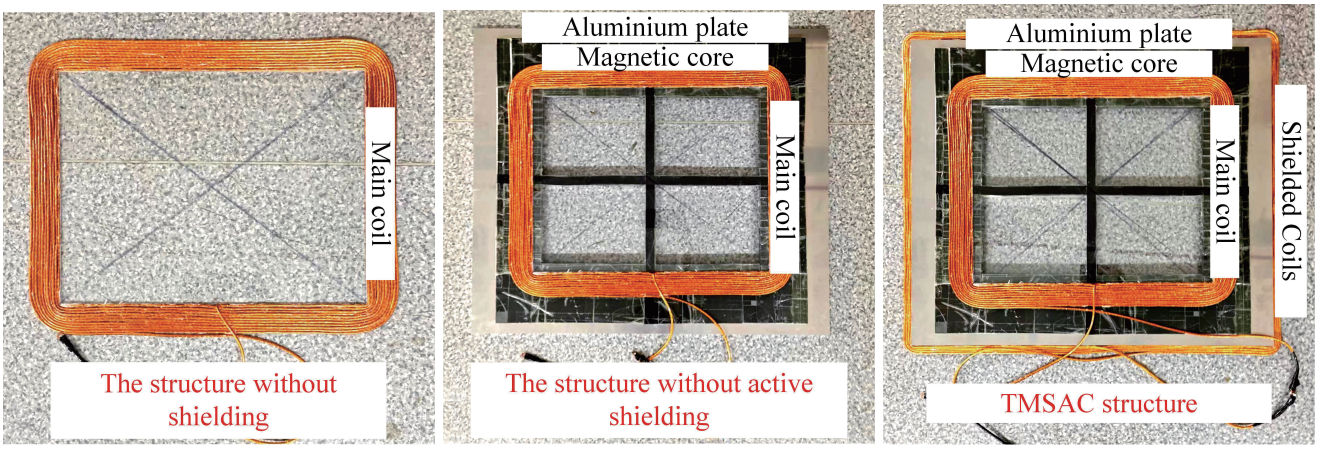

(a) (b) (c)

Fig. 17. Physical drawing of shielding structures. (a) The structure without shielding. (b) The structure without active shielding. (c) TMSAC structure.

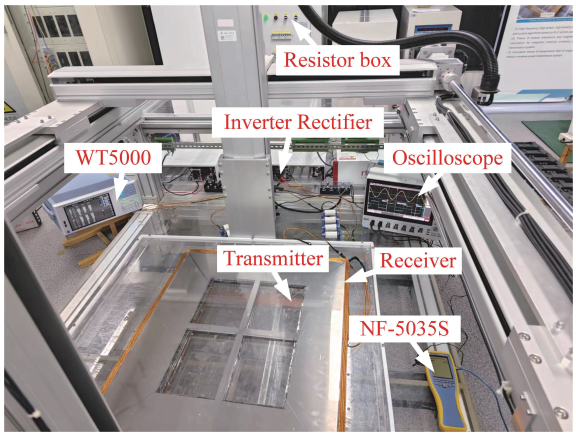

Fig. 18. Diagram of the overall framework of the experiment.

wound with leeds wire to reduce the internal resistance, with a specification of 0.1 mm × 800 strands and a maximum current of 31.415 A.

The experiment compares the magnetic leakage and transmission efficiency of three different structures to verify the effectiveness of the TMSAC structure, as shown in Fig. 17, which is the structure without shielding, the structure without active shielding, and the TMSAC structure.The overall framework of the experiment is shown in Fig. 18.

First, the physical characteristics of the coil structure were accurately measured using an IM3536 impedance analyzer, and the specific physical parameters of the resulting TMSAC structure are summarized in Table V. Subsequently, to assess the resonant state, the current and voltage waveforms at the transmitter and receiver of the coil were monitored by an oscilloscope, and the DC source voltage was adjusted accordingly to a suitable level to ensure that the output power was stabilized to 4 kW.

A. Magnetic Leakage of the System

Using Ansys Maxwell software, the simulation model of the TMSAC structure is drawn, and its simulation is performed to

TABLE V
PHYSICAL PARAMETERS OF THE TMSAC STRUCTURE

Parameter	Numerical value
Self-inductance of transmitter coil L_1/μH	225.15
Self-inductance of receiving coil L_2/μH	224.73
Resonant capacitance of transmitter coil C_1/nF	16.32
Resonant capacitance of receiving coil C_2/nF	16.27
Operating frequency f_0/kHz	85.00
Load R_L/Ω	24.00

obtain the simulated value of the maximum magnetic leakage B_s, finally, the experimental value of the maximum magnetic leakage B_e, of the target region of the TMSAC structure is measured by using the NF-5035S electromagnetic radiation analyzer, and the error between the simulated value and the experimental value is defined as ε_s, and the expression is:

$$\varepsilon_s=\frac{\left|B_S-B_e\right|}{B_e} \tag{16}$$

To verify the effectiveness of the TMSAC structure in reducing the magnetic leakage, the maximum magnetic leakage at the target region at the same offset is compared for the three structures of Fig. 18. The trend of the leakage magnetization with the offset distance of the receiving end is plotted, as shown in Fig. 19. The graph demonstrates the trend of a gradual increase in magnetic leakage with increasing offset distance.

After comparison, the magnetic leakage of the structure without active shielding is 33.27 μT at 10 cm offset, which is 81.01% less than that of the structure without shielding, and the TMSAC structure is 25.39 μT at 10 cm offset, which is 23.68% less than that the structure without active shielding, which conforms to the national standard, and the magnetic shielding performance of this structure is better than that of the structure without shielding and the structure without active shielding under the same size, and the validity of the designed

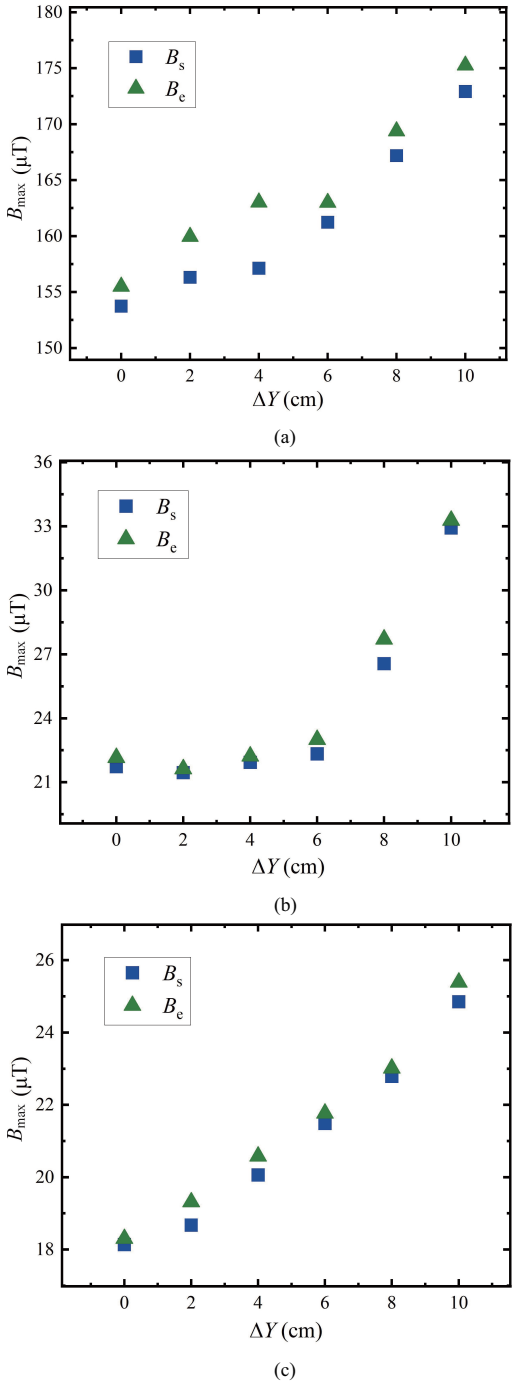

Fig. 19. Magnetic leakage for different shielding structures. (a) Magnetic leakage of the structure without shielding. (b) Magnetic leakage of the structure without active shielding. (c) Magnetic leakage of TMSAC structure.

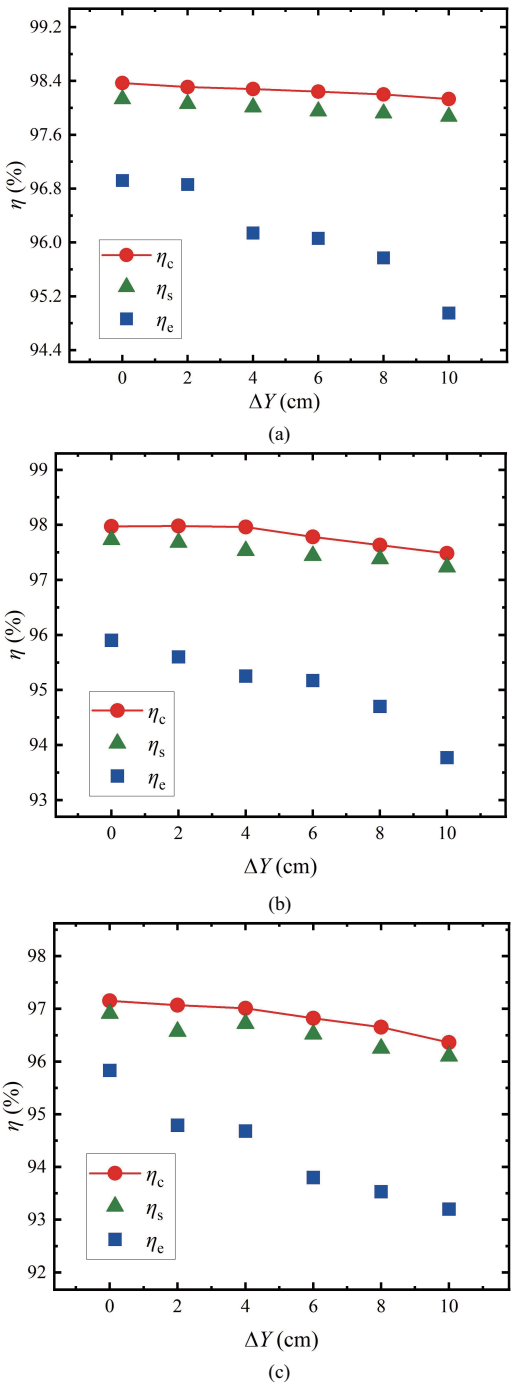

Fig. 20. Transmission efficiency for different shielding structures. (a) Transmission efficiency of the structure without shielding. (b) Transmission efficiency of the structure without active shielding. (c) Transmission efficiency of TMSAC structure.

structure and its method is verified.

B. Transmission Efficiency of the System

In this section, the transmission efficiency of three differ- ent structures at the same offset is compared to verify the effectiveness of the TMSAC structure. First, the theoretical transmission efficiency η_c is calculated based on (13) and (14), subsequently, the simulation efficiency η_s is obtained using MATLAB/Simulink, and finally, the experimental value of the system's transmission efficiency η_e is measured by the WT5000 power analyzer.

Fig. 20 shows the data curves of the transmission efficiency of the three structures with offset distance, which intuitively shows that the system efficiency decreases with the increase of offset, and the efficiency is reduced to the lowest at the offset of 10 cm. The experimental results show that the transmission efficiency of the TMSAC structure is as high as 95.83% under

TABLE VI
COMPARISON OF DIFFERENT EXISTING MAGNETIC SHIELDING SOLUTIONS

References	Shielding method	Material savings	B_z /μT	B_{xy}/μT	Efficiency/%
[26]	Fe	81.24% Magnetic core	More than 27	/	71.52
[27]	Fe	85.00% Magnetic core	73	/	91.00
[28]	Fe+Al	No savings	/	/	92.30
[29]	Fe+Al	No savings	/	14.40	91.20
[22]	Fe+Al+Active coil	No savings	/	15.35	92.60
[ourwork]	Fe+Al+Active coil	36.78% Magnetic core 32.52% Aluminum plate	18.13	0.95	95.83

the no-offset condition, and at an offset of 10 cm, its experimental transmission efficiency is only 1.84% lower than that of the structure without shielding, and 0.60% lower than that of the structure without active shielding. At the same offset distance,the transmission efficiency of the TMSAC structure is reduced by no more than 3% compared to the structure without shielding and the structure without active shielding. Moreover, it also highlights the advantage of the TMSAC structure, that is, even at the maximum offset of 10 cm, its efficiency remains high at 93.20%, and the theoretical transmission efficiency can be more than 95%.

Comparing the three structures, the transmission efficiency and the magnetic leakage in the target region at the same offset, it can be concluded that the TMSAC structure proposed in this paper has an excellent performance of magnetic leakage shielding in the perpendicular direction of the system and maintains a high transmission efficiency.

Comparison of the proposed structure with other WPT systems including shielding method, material saving rate, magnetic leakage after shielding and transmission efficiency is provided as shown in Table VI, where B_z denotes the magnetic leakage on the horizontal viewing surface above the receiving end and B_{xy} denotes the vertical viewing surface 80 cm from the center of the vehicle chassis. It shows that the proposed TMSAC structure has better electromagnetic shielding effect and transmission efficiency compared with other systems.

V. CONCLUSION

In this paper, a composite structure of Tian-font magnetic shielding and anti-series active coils is proposed, which has the significant advantage of realizing the saving of shielding materials while complying with the safety standards of magnetic leakage and maintaining a high transmission efficiency. In addition, a coil parameter optimization method is proposed, which solves the optimal parameter combinations of the main coil to meet the conditions based on the analysis of magnetic leakage and transmission efficiency. Based on the optimal parameters of the main coil, the factors affecting the magnetic leakage and transmission efficiency are analyzed to find the optimal material and shielding coil parameters. A physical experimental platform is further constructed, and the maximum magnetic leakage of the structure is measured to be 18.30 μT without offset, and the transmission efficiency is 95.83%, which reduces the magnetic leakage of 88.23% on the target region compared with the structure without shielding. Compared with the shielding structure of the same size, the magnetic core is saved by 36.78% and the aluminum plate is saved by 32.52%. In addition, at the maximum offset of 10 cm, the maximum magnetic leakage at the target region is 25.39 μT, which is still below 27 μT, and it is reduced by 23.68% compared with the structure without active shielding of the same size.

Through the optimized design, the structure successfully controls the maximum magnetic leakage of the upper 10 cm target region within the safety standard, ensuring high transmission efficiency while reducing the use of unnecessary materials, lowering the cost, and making it more economical and practical, which can be applied in the field of wireless charging of electric vehicles. In the future, the magnetic shielding structure needs to be further explored, and efforts should be made to reduce the complexity of the structure.

REFERENCES

[1] C. Liao, J. Li, and S. Li, "Design of LCC impedance matching circuit for wireless power transfer system under rectifier load," in *CPSS Transactions on Power Electronics and Applications*, vol. 2, no. 3, pp. 237–245, Sept. 2017.

[2] S. Y. R. Hui, "Past, present and future trends of non-radiative wireless power transfer," in *CPSS Transactions on Power Electronics and Applications*, vol. 1, no. 1, pp. 83–91, Dec. 2016.

[3] E. Abramov, I. Zeltser, and M. M. Peretz, "A network-based approach for modeling resonant capacitive wireless power transfer systems," in *CPSS Transactions on Power Electronics and Applications*, vol. 4, no. 1, pp. 19–29, Mar. 2019.

[4] Y. Zhang, S. Chen, X. Li, and Y. Tang, "Design of high-power static wireless power transfer via magnetic induction: An overview," in *CPSS Transactions on Power Electronics and Applications*, vol. 6, no. 4, pp. 281–297, Dec. 2021.

[5] B. Jiang, Z. Wang, Z. Yu, and M. Yuan, "Research on the measurement method of receive coil offset angle in MCR-WPT system," in *Journal of Electronic Measurement and Instrumentation*, vol. 37, no. 9, pp. 1–7, 2023.

[6] G. Rituraj, B. K. Kushwaha, and P. Kumar, "A unipolar coil arrangement method for improving the coupling coefficient without ferrite material in wireless power transfer systems," in *IEEE Transactions on Transportation Electrification*, vol. 6, no. 2, pp. 497–509, Jun. 2020.

[7] Y.-C. Hsieh, Z.-R. Lin, M.-C. Chen, H.-C. Hsieh, Y.-C. Liu, and H.- J. Chiu, "High-efficiency wireless power transfer system for electric vehicle applications," in *IEEE Transactions on Circuits and Systems II: Express*

Briefs, vol. 64, no. 8, pp. 942–946, Aug. 2017.

[8] J. Popović-Gerber, J. A. Oliver, N. Cordero, T. Harder, J. A. Cobos, M. Hayes, S. C. O' Mathuna, and E. Prem, "Power electronics enabling efficient energy usage: Energy savings potential and technological challenges," in *IEEE Transactions on Power Electronics*, vol. 27, no. 5, pp. 2338–2353, May 2012.

[9] L. Dong, F. Lin, C. Wang, and Q. Zhang, "Assessing human exposure to electromagnetic fields from catenary-free power supply urban rail transit vehicle," in *Transactions of China Electrotechnical Society*, vol. 36, no. S1, pp. 40–45, 2021.

[10] C. Chen, X. Huang, L. Tan, F. Wen, and W. Wang, "Electromagnetic environment and security evaluation for wireless charging of electric vehicles," in *Transactions of China Electrotechnical Society*, vol. 30, no. 19, pp. 61–67, 2015.

[11] D. E. Gaona, S. Ghosh, and T. Long, "Feasibility study of nanocrystalline-ribbon cores for polarized inductive power transfer pads," in *IEEE Transactions on Power Electronics*, vol. 35, no. 7, pp. 6799–6809, Jul. 2020.

[12] W. Zhang, Q. Yang, Y. Li, Z. Lin, M. Yang, and M. Mi, "Comprehensive analysis of nanocrystalline ribbon cores in high-power-density wireless power transfer pads for electric vehicles," in *IEEE Transactions on Magnetics*, vol. 58, no. 2, pp. 1–5, Feb. 2022.

[13] Q. Zhu, D. Chen, L. Wang, C. Liao, and Y. Guo, "Study on the magnetic field and shielding technique for an electric vehicle oriented wireless charging system," in *Transactions of China Electrotechnical Society*, vol. 30, no. S1, pp. 143–147, 2015.

[14] X. Fan, H. Zhang, F. Tang, and X. Zhang, "Investigation and application of electromagnetic metamaterials in the field of wireless power transfer," in *Proceedings of the CSEE*, vol. 42, no. 20, pp. 7623–7641, 2022.

[15] Z. Tian, J. Chen, J. Fan, Y. Lin, and W. Li, "The wireless power transfer system with magnetic metamaterials," *Transactions of China Electrotechnical Society*, vol. 30, no. 12, pp. 1–11, 2015.

[16] S. Kim, H.-H. Park, J. Kim, J. Kim, and S. Ahn, "Design and analysis of a resonant reactive shield for a wireless power electric vehicle," in *IEEE Transactions on Microwave Theory and Techniques*, vol. 62, no. 4, pp. 1057–1066, Apr. 2014.

[17] H. Moon, S. Kim, H. H. Park, and S. Ahn, "Design of a resonant reactive shield with double coils and a phase shifter for wireless charging of electric vehicles," in *IEEE Transactions on Magnetics*, vol. 51, no. 3, pp. 1–4, Mar. 2015.

[18] J. Meng, J. Tian, and M. Cai, "Research on active magnetic shielding for electric vehicle wireless power transfer system," in *Advanced Technology of Electrical Engineering and Energy*, vol. 40, no. 4, pp. 44–51, Nov. 2021.

[19] T. Campi, S. Cruciani, F. Maradei, and M. Feliziani, "Active coil system for magnetic field reduction in an automotive wireless power transfer system," in *Proceedings of 2019 IEEE International Symposium on Electromagnetic Compatibility, Signal & Power Integrity (EMC+SIPI)*, New Orleans, LA, USA, Jul. 2019, pp. 189–192.

[20] T. Campi, S. Cruciani, and M. Maradei, "Magnetic field mitigation by multicoil active shielding in electric vehicles equipped with wireless power charging system," in *IEEE Transactions on Electromagnetic Compatibility*, vol. 62, no. 4, pp. 1398–1405, Aug. 2020.

[21] S. Lee, D.-H. Kim, Y. Cho, H. Kim, C. Song, S. Jeong, J. Song, G. Park, S. Hong, J. Park, K. Cho, H. Lee, C. Seo, S. Ahn, and J. Kim, "Low leakage electromagnetic field level and high efficiency using a novel hybrid loop-array design for wireless high power transfer system," in *IEEE Transactions on Industrial Electronics*, vol. 66, no. 6, pp. 4356–4367, Jun. 2019.

[22] M. Mi, Q. Yang, Y. Li, P. Zhang, and W. Zhang, "Multi-objective active shielding coil design for wireless electric vehicle charging system," in *IEEE Transactions on Magnetics*, vol. 58, no. 2, pp. 1–5, Feb. 2022.

[23] M. Mohammad and S. Choi, "Optimization of ferrite core to reduce the core loss in double-D pad of wireless charging system for electric vehicles," in *Proceedings of 2018 IEEE Applied Power Electronics Conference and Exposition (APEC)*, Mar. 2018, pp. 1350–1356.

[24] P. L. X. J. W. Li, Z. and H. Liu, "Leakage magnetic field calculation and optimization of double inverse series coil structure of electric vehicle wireless charging systems," in *Progress In Electromagnetics Research B*, vol. 96, pp. 213–233, 2022.

[25] Z. Chen, Z. Li, Z. Lin, J. Li, and Y. Zhang, "Mutual inductance calculation of rectangular coils at arbitrary position with bilateral finite14 magnetic shields in wireless power transfer systems," in *IEEE Transactions on Power Electronics*, vol. 39, no. 10, pp. 14065–14076, Oct. 2024.

[26] G. Rituraj and P. Kumar, "A new magnetic structure of unipolar rectangular coils in WPT systems to minimize the ferrite volume while maintaining maximum coupling," in *IEEE Transactions on Circuits and Systems II: Express Briefs*, vol. 68, no. 6, pp. 2072–2076, Jun. 2021.

[27] M. G. S. Pearce, G. A. Covic, and J. T. Boys, "Reduced ferrite double D pad for roadway IPT applications," in *IEEE Transactions on Power Electronics*, vol. 36, no. 5, pp. 5055–5068, May 2021.

[28] R. Qin, J. Li, J. Sun, and D. Costinett, "Shielding design for high frequency wireless power transfer system for EV charging with selfresonant coils," in *IEEE Transactions on Power Electronics*, vol. 38, no. 6, pp. 7900–7909, Jun. 2023.

[29] M. G. S. Pearce, G. A. Covic, and J. T. Boys, "Robust ferrite-less double D topology for roadway IPT applications," in *IEEE Transactions on Power Electronics*, vol. 34, no. 7, pp. 6062–6075, Jul. 2019.

Zhongqi Li was born in China, in 1985. He received the M.Sc. degree from Hunan University of Technology, Zhuzhou, China in 2012, and the Ph.D. degree from the Hunan University, Changsha, China, in 2016.

From 2016, he is currently working as an Assistant Professor with Hunan University of Technology, Zhuzhou, China. From 2020, he is currently working as a Postdoctoral Fellow with Hunan University, Changsha, China. His research interests include wireless power transfer systems and soft-switching power converters.

Wenjuan Zhang was born in China, in 2001. She received a bachelor's degree in electronic information engineering from Wuyi University, Fujian, China, in 2023. She is currently pursuing the Master's degree in control theory and control engineering at Hunan University of Technology. Her current research interests include wireless power transfer systems.

Ziyue Gan was born in China, in 1999. She received a bachelor's degree in electrical engineering and automation from Hunan University of Engineering, Hunan, China, in 2021. She is currently pursuing the Master's degree in energy power at Hunan University of Technology. Her current research interests include wireless power transfer systems.

Bin Li was born in China, in 2000. He received a bachelor's degree in electrical engineering and automation from Hunan University of Technology, Hunan, China, in 2022. He is currently pursuing the Master's degree in electrical engineering at Hunan University of Technology. His current research interests include wireless power transfer systems.